

Sulphydryl-Functionalized Amino Group Polymer Microcomposites toward Efficient Adsorption of Aqueous Cr(VI), As(III), Cd(II), and Pb(II)

Yueyang Wang,[#] Weiwei Lu,[#] Fangfen Jing, Mingzhu Jin, Xinyang He, Yuchen Xue, Yajun Hu, and Rongtai Yu*



Cite This: *Langmuir* 2024, 40, 519–528



Read Online

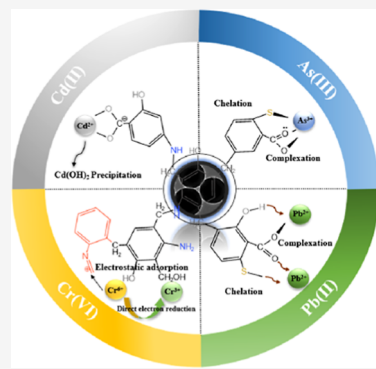
ACCESS |

Metrics & More

Article Recommendations

Supporting Information

ABSTRACT: The development of efficient adsorbents for heavy metal pollution, especially five toxic heavy metals, has attracted great research interest. Polymer-based adsorbents have aroused research value for their abundant functional groups and high porosity to the ability to capture metal ions. We designed a sulphydryl-functionalized polymer microcomposite to take up Cr(VI), As(III), Cd(II), and Pb(II). The adsorption capacity achieved was 64.2 mg g⁻¹ for Cr(VI), 44.9 mg g⁻¹ for As(III), 35.5 mg g⁻¹ for Cd(II), and 18.2 mg g⁻¹ for Pb(II). Langmuir and Sips isotherm model is dominant for As(III), Cd(II), and Pb(II) adsorption. Pseudo-second-order kinetic models can better describe the adsorption behavior of Cr(VI), implying that chemisorption is accompanied by Cr(VI) adsorption. Cr(VI) simultaneous reduction to Cr(III) through the benzenoid amine oxidate pathway was the dominant mechanism, precipitation for Cd(II) adsorption was convinced, and chelation between As(III)/Pb(II) and—SH group and complexation between Pb(II) and C=O or benzene hydroxyl were a plausible mechanism for As(III) and Pb(II) adsorption.



INTRODUCTION

Polymer, a new family of materials, was named by Swedish chemist J. J. Berzelius emerged in the 1920s.¹ The discovery of polymers challenged traditional materials. Until now, more and more synthetic polymer methods are emerging. New polymer species and morphology, like phenolic resin, were commercialized.² It is interesting to note that polymer-based nanocomposites have aroused great attention for pollutant adsorption due to the nature of polymer constituents, distribution, and properties. Polymer-based nanocomposites, for their environmentally harmless nature and degradability, have great potential for environmental application. A large number of adsorbents have been applied to sewage treatment. Activated carbon, the most representative adsorbent, has the disadvantages of saturation capacity limitation, poor selectivity, and poor reproducibility.^{3–5} However, the shortage of bleak surface functional groups results in poor adsorption efficiency for existing adsorbents, even for nanocomposite materials. The poor adsorption capacity and selectivity of the polymer nanocomposite hinder its application.

Surface functional treatments are considered an effective strategy to improve the adsorption capacity of polymer nanocomposites at the solid–liquid interface adsorption. Recent studies showed that functional counterparts can provide targeted adsorption sites for specific pollutants. For example, Elwakeel et al. have achieved the recovery of Cu(II), Cd(II), and Pb(II) by functionalization of polyacrylonitrile/Na-Y-zeolite composite with amidoxime groups.⁷ Wieszc-

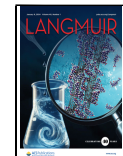
zycka et al. pointed out that the efficiency of Cu(II), Zn(II), and Cd(II) adsorption depended on the functional group during Cu(II), Zn(II), and Cd(II) adsorption by the porous organic poly copolymer modified using quaternization with 1-undecan-1-one and 1-ethan-1-one.⁸ The disadvantages of polymer nanocomposites, like poor adsorption capacity and aggregation, can be improved by grafted functional groups. As reported in the literature, polymers with incorporated functional counterparts have been demonstrated as ideal adsorbents.^{9,10} To fulfill the goal, sulphydryl-grafted grafted materials arouse research enthusiasm. Li et al. have achieved Pb(II) and Cd(II) adsorption by chitosan/sulphydryl-graphene oxide composite.¹¹ Ye et al. and Cao et al. believed that the chelation between As(III)/Cd(II) and—SH groups was the key mechanism using chitosan and ion-imprinted polymer as adsorbents.^{12,13} It implies that the sulphydryl functional group has a natural advantage for Pb(II), Cd(II), and As(III) removal. Meanwhile, amino groups have been confirmed to have a strong affinity for Cr(VI) reduction by electron-donating of amine to imine.¹⁴ It is fascinating to hold

Received: September 15, 2023

Revised: December 7, 2023

Accepted: December 7, 2023

Published: December 27, 2023



sulphydryl and amine functional groups on an adsorbent and use it for performance adsorption in the environmental field.

Phenolic resin polymers, with unique physical and chemical properties, like size, shape, surface charge, and porosity, are enthusiastically appealing for potential applications as adsorbents and exhibit excellent catalytic performance.¹⁵ The synthesis of phenolic resin polymers that precisely controlled the size of the spheres presents great challenges.^{16,17} The popular stÖber synthesis method originated from silica spheres with sol–gel formation. The similarity pattern of polymerization for phenolic resin was successfully prepared by the stÖber method.¹⁸ Furthermore, heavy metal pollution is one of the research hotspots in the environmental field, especially Cr(VI), As(III), Cd(II), and Pb(II), four of the five heavy metals, which are discharged into natural water bodies by the industry or other means, posing significant potential harm to human health and the ecological environment. Drinking water containing heavy metals can cause serious health problems, like liver, kidney, etc. The study of heavy metal treatment is urgent.^{19–23} Therefore, a resin stÖber polymer sphere functionalized by grafted sulphydryl groups was used to investigate the removal of toxic Cr(VI), As(III), Cd(II), and Pb(II) from aqueous. The adsorption capacity and effectiveness were studied, and the effect of pH, metal ions' initial concentration, isotherms, kinetics, and adsorbent dosage was carried out; the mechanism and competitive adsorption were also explored.

MATERIALS AND METHODS

Chemicals. 3-Aminophenol (3-AP, 98%), formaldehyde solution (37 wt %), ammonia aqueous solution (NH_4OH , 25 wt %), potassium dichromate ($\text{K}_2\text{Cr}_2\text{O}_7$, A.R.), arsenic trioxide (As_2O_3 , A.R.), lead nitrate ($\text{Pb}(\text{NO}_3)_2$, A.R.), and 4-aminothiophenol ($\text{C}_6\text{H}_5\text{NS}$, A.R.) were ordered from Aladdin (Shanghai, China), and acetone ($\text{C}_3\text{H}_6\text{O}$, 97 wt %), cadmium chloride, (CdCl_2 , A.R.), and all the other chemicals used in this work were purchased by Sinopharm Group (China). All chemicals were used as obtained without further purification.

Synthesis and Modification of Resin stÖber Spheres. *Phenolic Resin Spheres Synthesis.* The stÖber method was used to prepare resin spheres by a slight modification. Typically, 0.1 g of 3-AP, 0.1 mL of formaldehyde solution, and 0.05 mL of NH_4OH were added to a flask with 30 mL of deionized water, and the mixed solution was stirred for 20 min at ambient temperature. Then, the colloidal suspension was obtained and thoroughly washed with deionized water three times, followed by freeze-drying for 48 h.²⁴

Sulphydryl Grafting. Sulphydryl-functionalized resin polymers were prepared by the method reported by Li et al.¹¹ First, 12 mmol of 4-amino thiophenol and 1 N HCl were poured into a 250 mL flask, and the mixture was slowly heated to 53 °C under continuous stirring. Then, the solution was cooled in an ice bath. After that, 12 mmol of NaNO_2 (20 mL) was added to the above solution drop by drop under agitating. Finally, 1 g of the collected resin stÖber spheres and 200 mL of distilled water were added to the above-mixed solution while stirring constantly under an ice bath for 12 h. The modified product was collected by centrifugation and washed with ethanol and deionized water.

Adsorption Procedures. Adsorption Experiments. Cr(VI), As(III), Cd(II), and Pb(II) adsorption experiments were carried out in a 10 mL serum bottle containing 4 mL of mixed solution, which included metal ions and the adsorbent. Typically, 0.1 mg/mL modified product was introduced into a 10 mL serum bottle including a designed concentration of metal ions with a specified pH value; the pH value was not adjusted throughout the whole experiment. 2 mL of the mixed solution was sampled out and centrifugated for subsequent analysis. Cr^{6+} and As^{3+} ion concentrations were measured by spectrophotometry, while Cd^{2+} and Pb^{2+} were analyzed by EDTA

chemical titration. Cd^{2+} and Pb^{2+} concentrations were calculated by the following equation.

$$c_{\text{Cd},\text{Pb}} = \frac{C_{\text{EDTA}} V_{\text{EDTA}} \times M_{\text{Cd},\text{Pb}}}{V_{\text{Pb,Cd}}} \quad (1)$$

where $C_{\text{Cd},\text{Pb}}$ (g L^{-1}), $M_{\text{Cd},\text{Pb}}$, and $V_{\text{Cd},\text{Pb}}$ (L) are the mass concentration, molar weight, and volume of Cd(II) and Pb(II), and C_{EDTA} (mol L^{-1}) and V_{EDTA} (L) are the molar concentration and consumed volume of EDTA standard solution, respectively. All of the experiments were investigated in duplicate, and error bars were calculated in all figures.

In the competitive adsorption part, one metal ion coexisted with the other metal ions in a binary solution. The experiments were designed to change one metal ion concentration from 1 to 20 mg L^{-1} ; the other metal ion concentration was maintained at a constant value of 20 mg L^{-1} for As(III) and Pb(II) and 50 mg L^{-1} for Cr(VI) and Cd(II), respectively. The other parameters were the same as those in the above experiment.

Modeling Methods. Isotherm models can predict the surface properties and affinity of the adsorbent at equilibrium.¹⁴ Langmuir, Freundlich, and Sips models were used in this study. The nonlinear forms of these models are presented in the following, respectively.

$$q_e = q_{\max} \frac{K_L C}{1 + K_L C} \quad (2)$$

$$q_e = K_F C^{1/n} \quad (3)$$

$$q_e = q_{\max} \frac{(K_S C)^{\gamma}}{1 + (K_S C)^{\gamma}} \quad (4)$$

where q_{\max} is the maximum adsorbate adsorption capacity (mg g^{-1}), C is the equilibrium adsorbate concentration (mg L^{-1}), q_e is the amount of adsorbate at equilibrium (mg g^{-1}), K_L and K_F are the Langmuir constant (L mg^{-1}) and Freundlich constant ($\text{mg}^{1-(1/n)} \text{ L}^{1/n} \text{ g}^{-1}$), respectively, n represents the Freundlich parameter, K_S is the equilibrium constant, and γ is a dimensionless exponent.^{25,26}

Adsorption kinetics can predict the adsorption process and mechanism and even the possible rate-limiting steps. Cr(VI), Cd(II), As(III), and Pb(II) adsorption on the modified polymer micro-composites were described by pseudo-first-order, pseudo-second-order, and Elovich models. The linearized form of these two models is presented in eqs 5, 6, and 7, respectively.^{14,25}

$$\log q_e - q_t = \log q_e - k_1 t \quad (5)$$

$$\frac{t}{q_t} = \frac{1}{k_2 q_e^2} + \frac{t}{q_e} \quad (6)$$

$$\left(\frac{dq_t}{dt} \right) = \alpha \exp(-bqt) \quad (7)$$

where q_e is adsorbate equilibrium adsorption capacity (mg g^{-1}), q_t is the amount of adsorbate at time t (min), k_1 and k_2 are pseudo-first-order and pseudo-second-order rate constants, and α and b are constants.²⁷

The thermodynamic parameters of the standard free energy (ΔG°), enthalpy (ΔH°), and entropy (ΔS°) are calculated with the following equation.

$$\Delta G^\circ = -RT \ln K_c \quad (8)$$

$$\Delta G^\circ = \Delta H^\circ - T \Delta S^\circ \quad (9)$$

$$\ln K_c = -\Delta H^\circ / RT + \Delta S^\circ / R \quad (10)$$

$$K_c = C_\alpha / C_e \quad (11)$$

Equation 8 is also named as van't Hoff equation, where $T(K)$ is the ambient temperature, R is 8.314 J/(mol K), and K_c , C_α , and C_e are the standard thermodynamic equilibrium constants, the concentration of

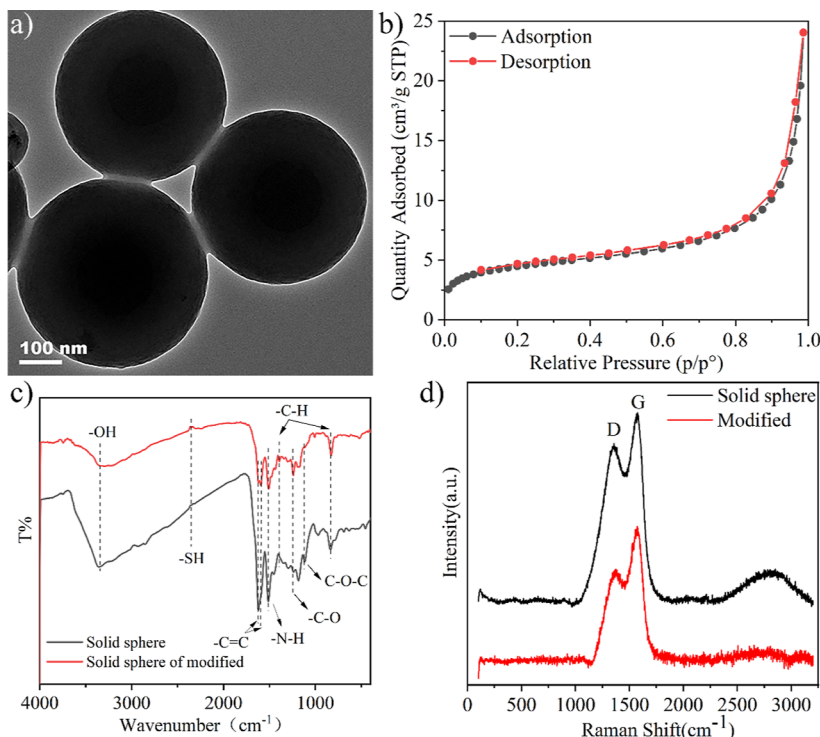


Figure 1. Structure characterization of the sulfhydryl-functionalized polymer particles. (a) TEM images; (b) N_2 adsorption–desorption isotherms; (c) FTIR spectra; and (d) Raman spectrum.

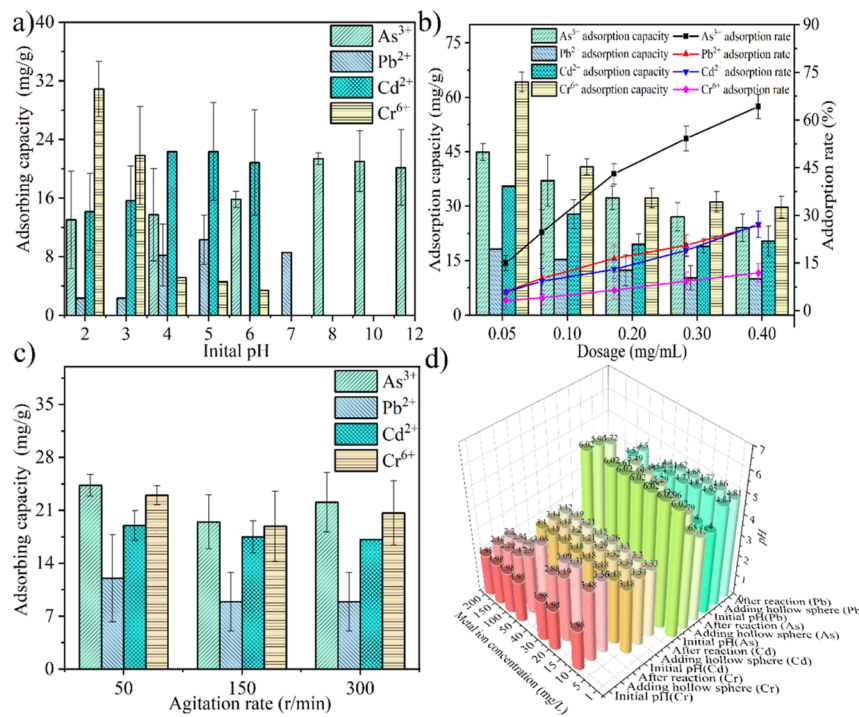


Figure 2. Adsorption performances of the sulfhydryl-functionalized polymer particles. The effect of initial pH (a) and dosage (b) on the adsorption capacities. Agitation rate (c) and pH vary under different conditions (d).

adsorbed ions, and residual concentration in the supernate, respectively.^{28,29}

Characterization. Scanning electron microscopy was recorded on a SU-8010, and transmission electron microscopy was conducted using JEOL JSM 2010. Nitrogen sorption analysis was acquired on an ASAP 2460 at 250 °C. X-ray photoelectron spectroscopy was obtained by a Thermo Scientific Escalab 250 Xi, and Fourier transform infrared

(FTIR) spectra were recorded on a Thermo Nicolet 5700 spectrometer. Raman spectra were investigated by Renishaw in a Via Qontor.

RESULTS AND DISCUSSION

Characterization of the Sulfhydryl-Functionalized Polymer Particles. A solid inside rather than gelled particles

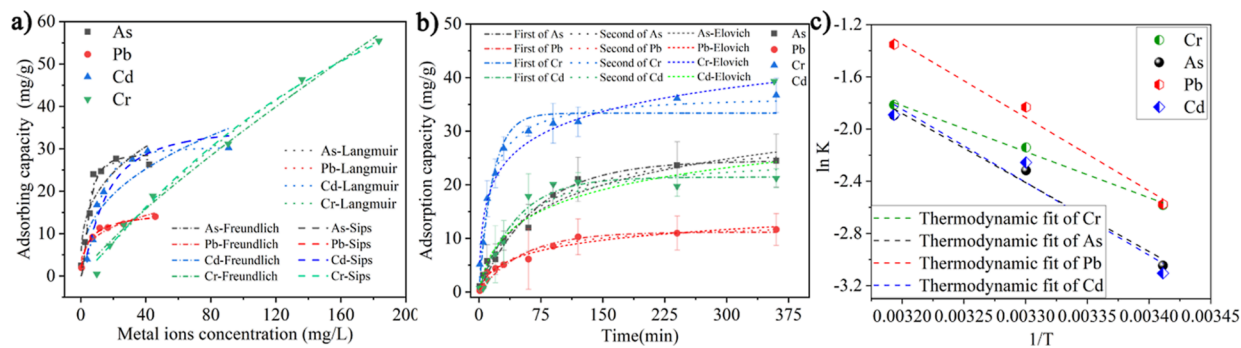


Figure 3. Adsorption isotherm, kinetics, and thermodynamics. Langmuir and Freundlich isotherm models and (a) pseudo-first-order and pseudo-second-order and (b,c) plotted curves of $\ln K$ with $1/T$.

Table 1. Adsorption Isotherm Parameters of the Sulfhydryl-Functionalized Polymer Particles

| | isotherms | | | | | | | | | | | |
|---------|------------|-------|-------|------------|-------|-------|------------|-------|----------|-------|--|--|
| | Langmuir | | | Freundlich | | | Sips | | | | | |
| | q_{\max} | K_L | R^2 | $1/n$ | K_F | R^2 | q_{\max} | K_s | γ | R^2 | | |
| Cr(VI) | 128.53 | 0.02 | 0.99 | 0.84 | 0.72 | 0.99 | 115.65 | 0.005 | 1.12 | 0.99 | | |
| Cd(II) | 30.48 | 0.17 | 0.98 | 0.27 | 9.89 | 0.76 | 35.70 | 0.07 | 1.36 | 0.95 | | |
| As(III) | 27.66 | 0.32 | 0.96 | 0.32 | 9.28 | 0.80 | 28.92 | 0.20 | 1.98 | 0.95 | | |
| Pb(II) | 16.01 | 0.72 | 0.99 | 0.37 | 3.66 | 0.84 | 16.01 | 0.21 | 0.80 | 0.99 | | |

Table 2. Adsorption Kinetic Parameters of the Sulfhydryl-Functionalized Polymer Particles

| | kinetics | | | | | | | | | | | |
|---------|--------------------------|-----------------------|-------|---------------------------|-----------------------|-------|---------------|---------|-------|--|--|--|
| | pseudo-first-order model | | | pseudo-second-order model | | | Elovich model | | | | | |
| | q_e | k_1 | R^2 | q_e | k_2 | R^2 | α | β | R^2 | | | |
| Cr(VI) | 33.36 | 2.77×10^{-3} | 0.95 | 36.87 | 2.96×10^{-7} | 0.98 | 8.99 | 0.16 | 0.96 | | | |
| Cd(II) | 27.81 | 5.56×10^{-3} | 0.97 | 21.44 | 1.81×10^{-5} | 0.94 | 0.88 | 0.16 | 0.90 | | | |
| As(III) | 44.55 | 3.18×10^{-4} | 0.96 | 78.58 | 4.62×10^{-4} | 0.96 | 0.70 | 0.14 | 0.97 | | | |
| Pb(II) | 16.77 | 3.4×10^{-2} | 0.96 | 27.5 | 1.0×10^{-3} | 0.95 | 0.50 | 0.34 | 0.97 | | | |

was observed after phenolic resin polymerization, which have uniform particle sizes of approximately 450 nm (Figures 1a and S1, Supporting Information). There is a complicated inhomogeneous nature composition distribution inside single nanoparticles. Therefore, a wide variety of architectures, including concave, hollow, and multishelled particles, were designed by acetone etching, and its unprecedentedly high adsorption capacity was proposed by the exposure of the surface functional groups.^{24,30} N₂ adsorption–desorption analysis results revealed that nanopores were present in the solid particles for a type IV behavior and hysteresis loops. 16.38 m²/g of the Brunauer–Emmett–Teller (BET) surface area and 0.034 cm³ g⁻¹ of total pore volume were recorded for the sulfhydryl-functionalized polymer particles (Figure 1b). It implies that the resin stÖber spheres are not completely solid inside; nanopores will increase the specific surface area and adsorption capacity.

The groups of –N–H stretching vibration at 1510 cm⁻¹ come from intrinsic 3-aminophenol, the precursor of the sulfhydryl-functionalized polymer particles (Figure 1c). The peak of –N–H stretching vibration at 1510 cm⁻¹ was assigned to benzenoid amine, and –C=C stretching at 1623 cm⁻¹ can be attributed to the stretching vibrations of quinoid imine.³¹ The peaks of –C–H stretching at 1427 and 833 cm⁻¹, –O–C stretching at 1232 cm⁻¹, and C–O–C stretching at 1110 cm⁻¹ originated from the polymer.²⁴ A new peak of the –S–H stretching band at 2347 cm⁻¹ was observed after modification,

implying that the –S–H groups were grafted on the surface of the polymers.¹¹ The peak strength of broad band at 3328 cm⁻¹ assigned to –OH groups and the peak of benzenoid amine/quinoid imine decreased obviously after sulfhydrylation, indicating that the sulfhydryl group may be attached to the benzenoid amine/quinoid imine or the benzene hydroxyl groups. Raman spectroscopy results showed that the I_D/I_G ratio was 1:1.1 and 1:1.6 for the pristine polymers and modified polymers, respectively (Figure 1d). D peak and G peak were attributed to quinoid imine and benzenoid amine, respectively.³² The decrease in I_D/I_G ratio further suggests that the grafted sulfhydryl group is possibly grafted to benzenoid amine groups or other groups, and the steric hindrance of quinoid imine/benzenoid amine groups is changed, which leads to a decrease in the I_D/I_G ratio.

Adsorption Performance of the Sulfhydryl-Functionalized Polymer Particles. Effect of pH on the Adsorption Performance of the Sulfhydryl-Functionalized Polymer Particles. H⁺ ions would compete with metal ions like Cd²⁺ and Pb²⁺ during the adsorption process. The surface charge of the adsorbent changes as a function of pH for the point of zero electric charge (PZC), which is attributed to surface functional groups, deprotonation, and even the nature of the polymer. As shown in Figure 2a, Cr(VI) adsorption capacity fell sharply as the initial pH rose from 30.9 mg g⁻¹ at pH 2 to 3.4 mg g⁻¹ at pH 6. Interestingly, for similar ionic states, the curve of Cd(II) and Pb(II) adsorption capacity has similar changes, which go

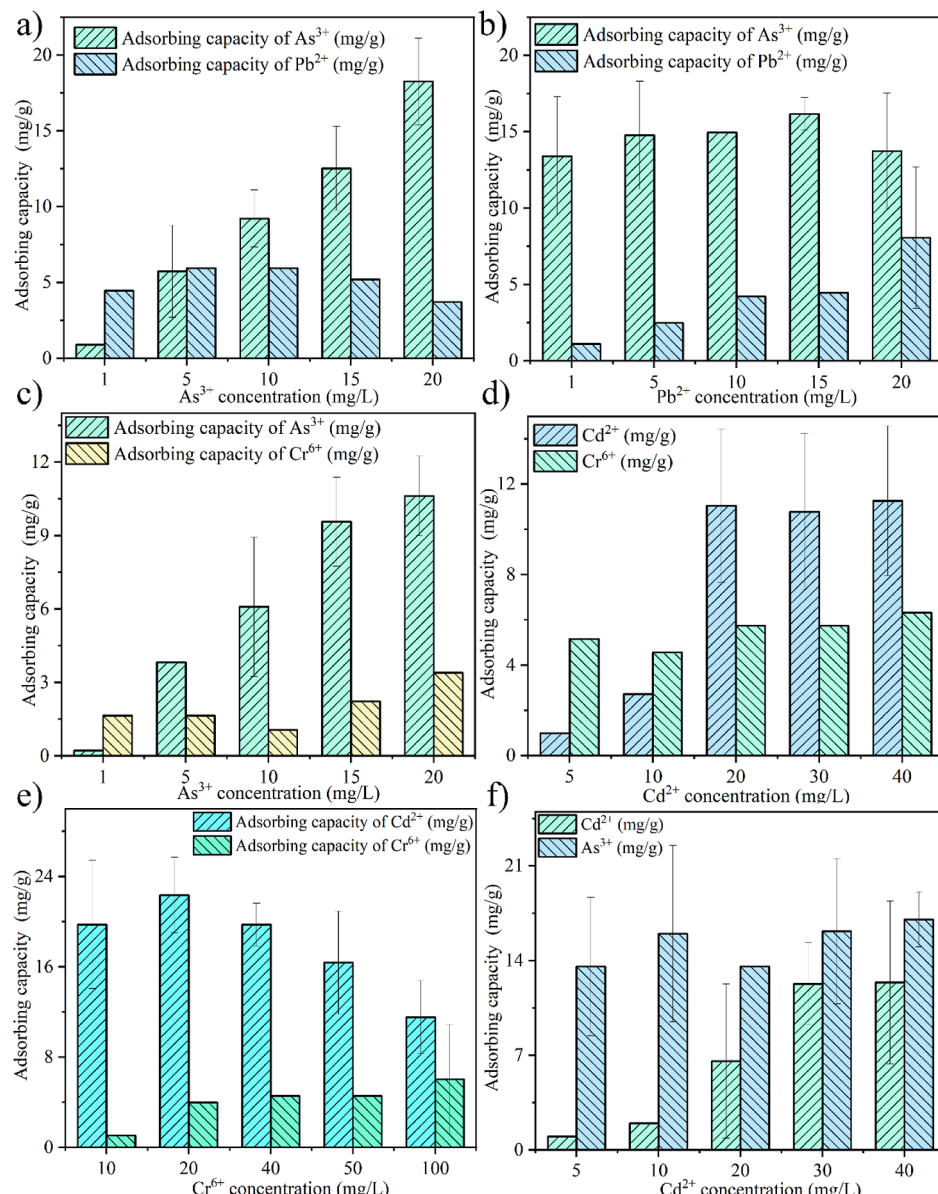


Figure 4. Competitive adsorption behaviors: (a) Pb(II) 20 mg L⁻¹; (b) As(III) 20 mg L⁻¹; (c) Cr(VI) 50 mg L⁻¹; (d) Cr(VI) 50 mg L⁻¹; (e) Cd(II) 30 mg L⁻¹; and (F) As(III) 20 mg L⁻¹.

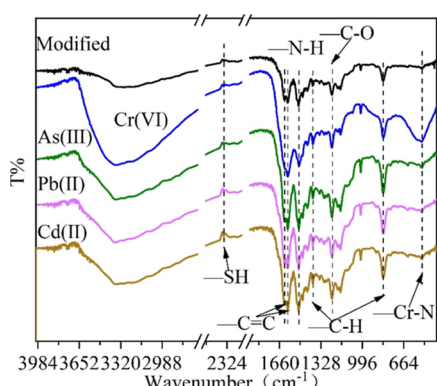


Figure 5. FTIR spectra of the sulphydryl-functionalized polymer particles after metal ion adsorption.

up then down; the optimal pH value was 5. However, the adsorption capacity of As(III) is unusual as the function of pH

for the special properties of As(III), which improved slowly as pH rose, then achieved the highest at pH 8.

When pH is below 6, the surface of the polymer is positively charged in our previous report, and there is a negative charge at pH above 7.²⁴ H₃AsO₃⁻ is the predominant species at a pH below 9.2 and H₂AsO₃²⁻ at pH 9.3–14.³³ Cr(VI) species presented in a state of negatively charged ions, HCrO₄⁻ is dominated at pH below 5, while CrO₄²⁻ is predominated at pH above 6.46.²² Although Cr(VI) and As(III) have similar ionic states at alkaline conditions, the adsorption process is completely different. HCrO₄⁻ species has a higher adsorption capacity at pH 2 by electrostatic adsorption. The adsorption capacity of H₃AsO₃⁻ was higher at pH above 9 with electrostatic repulsion conditions, implying that the mechanism of As(III) was mainly attributed to the surface functional groups. The surface charge of the sulphydryl-functionalized polymer is positive under acidic conditions, while Cd(II) and Pb(II) are also positively charged, electrostatic repulsion is inevitable between Cd(II)/Pb(II) species and the sulphydryl-function-

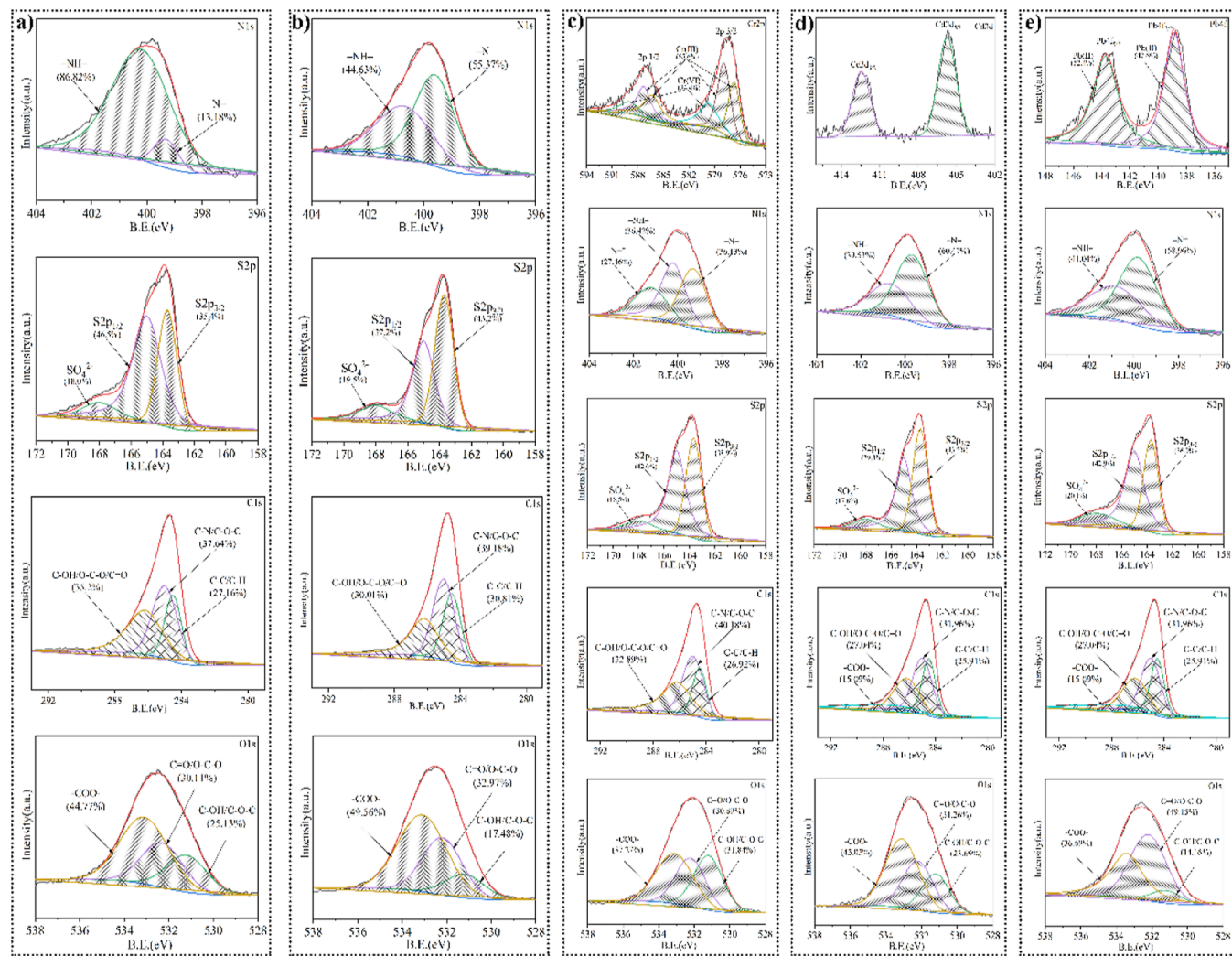


Figure 6. XPS analysis results of the sulphydryl-functionalized polymer particles (a). After As(III) adsorption (b). After Cr(VI) adsorption (c). After Cd(II) adsorption (d) and (e) after Pb(II) adsorption.

alized polymer. It implies that the mechanism of Cd(II)/Pb(II) adsorption by the polymer is related to exchange or chelation.

Effect of Dosage and Agitation Rate. The adsorption capacity decreased when the dosage was from 0.05 to 0.4 mg mL⁻¹, with an adsorption capacity of 64.2, 44.9, 35.5, and 18.2 mg g⁻¹ for Cr(VI), As(III), Cd(II), and Pb(II) at the dosage of 0.05 mg mL⁻¹, respectively (Figure 2b). The affinity of the sulphydryl-functionalized polymer was Cr(VI) > As(III) > Cd(II) > Pb(II). More adsorption sites are provided when the dosage increases, and the surplus of available adsorption sites causes a decrease in adsorption efficiency. Stirring increases the chance of contact between adsorbent and adsorbate, while rapid stirring will break the weak force resulting in adsorption capacity decrease. The adsorption capacity was at best at 50 r min⁻¹, whether for Cr(VI), As(III), or Cd(II), Pb(II) (Figure 2c). The adsorption capacity was slightly decreased with the increase in stirring speed, implying that agitation affects the interaction between Cr(VI), As(III), Cd(II), Pb(II), and the sulphydryl-functionalized polymer. Therefore, the stirring speed was 50 r min⁻¹ for further studies.

The change in pH is intrinsic to the mechanism during the adsorption reaction. The pH value was measured before and after adsorption at different metal ions' initial concentrations.

The results indicated that the pH value declined gradually after introducing the sulphydryl-functionalized polymer, from 3.21 to 3.15 for Cd(II), from 5.61 to 5.49 for As(III), and from 4.54 to 4.4 for Pb(II) at 30 mg L⁻¹ (Figure 2d). Interestingly, the pH value slightly rises after the adsorption reaction of Cr(VI), from 2.88 to 3.09 at 30 mg L⁻¹, whereas, due to the substitution of hydrogen ions by As(III), Cd(II), and Pb(II) species, it results in a drop in pH after adsorption. It implies that ion change or complexation was inevitable between As(III), Cd(II), Pb(II) ions, and benzene hydroxyl, carboxylic, or sulphydryl groups. However, a unique mechanism is plausible for Cr(VI) adsorption. The protonation of quinoid imine and reduction reaction of Cr(VI) to Cr(III) consume H⁺ ions, which cause the pH value to rise, implying that quinoid imine is the instinct of Cr(VI) adsorption by the sulphydryl-functionalized polymer.³⁴

Adsorption Isotherms, Kinetics, and Thermodynamic Analysis. The equilibrium data for Cr(VI), As(III), Cd(II), and Pb(II) extractions are shown in Figure 3a. Langmuir, Sips, and Freundlich models were used to describe the behavior of metal ions by the sulphydryl-functionalized polymer particles, and the calculation parameters are presented in Table 1. The dosage of 0.3 mg mL⁻¹ was used in isotherm and kinetic experiments for more accurate data, which caused the

theoretical calculation of adsorption capacity to be lower than the experimental value. A higher correlation coefficient ($R^2 > 0.95$) indicates that the equilibrium data of As(III), Cd(II), and Pb(II) adsorption fit the Langmuir and Sips isotherm model better than the Freundlich models. The Langmuir isotherm model is based on monolayer adsorption, which depicts chemisorption with identical binding sites.^{35,36} Sips predicts heterogeneous adsorption and monolayer adsorption at high concentrations.³⁷ The Langmuir and Sips isotherm models suggest that the mechanism for As(III), Cd(II), and Pb(II) adsorption is mainly chemisorbed, which fits perfectly with the experimental data. However, based on the R^2 value, Langmuir, Sips, and Freundlich isotherm models coexisted during Cr(VI) adsorption. Langmuir and Sips isotherms depict chemisorption, while the Freundlich model is related to physisorption. That is to say, chemisorption and physisorption occurred simultaneously for Cr(VI) adsorption, implying that a redox reaction is confirmable. Freundlich isotherm models with multilayer adsorption on heterogeneous surfaces described the electrostatic adsorption process during Cr(VI) uptake. The Langmuir constant (K_L) value and the Freundlich parameter $1/n$ provide insight into the favorability of adsorption, where $K_L > 0$ and $1/n$ close to 0 indicates favorable adsorption.^{36,38} Based on the data in Table 1, chemisorption is dominant for Cr(VI) adsorption by the sulphydryl-functionalized polymer particles.

The reaction pathways can be described by the pseudo-first-order, Elovich, and pseudo-second-order kinetic models; the linear form and fitted data are shown in Figure 3b and Table 2. A fast stage at the first 60 min was achieved for Cr(VI) adsorption, while it takes approximately 120 min for As(III), Cd(II), and Pb(II) adsorption (Figure 3b). The higher R^2 for Cr(VI) adsorption suggests that pseudo-second-order and Elovich kinetic models can better describe the adsorption behavior of Cr(VI). Pseudo-second-order and Elovich kinetic models described the nature of chemisorption, implying that chemisorption is predominant for Cr(VI), and the conclusion agrees with the experimental data and the results of adsorption isotherms. The very close R^2 value for As(III) and Pb(II) adsorption suggests that pseudo-first-order, Elovich, and pseudo-second-order kinetic models also fit the data during the adsorption process, implying that ion exchange between As(III) and Pb(II) ions and –SH groups or –OH groups are presented, and physisorption simultaneous existed; the results agree with the data of pH change and isotherms. The R^2 value of Elovich and pseudo-second-order kinetic models for Cd(II) adsorption is less than 0.95, while the R^2 value of pseudo-first-order is 0.97, which indicates that the pseudo-first-order model is the primary adsorption mechanism for Cd(II) adsorption.

The thermodynamic results are shown in Figure 3c, and ΔH° and ΔS° can be achieved from the slope and intercept of the plotted curves, respectively. The calculated values of ΔG° , ΔH° , and ΔS° are shown in Table S1. The positive values of ΔH° for Cr(VI), As(III), Cd(II), and Pb(II) reveal that adsorption is an endothermic process; the higher ΔH° values of As(III), Cd(II), and Pb(II) indicated that they need to absorb more heat than Cr(VI). The increase in randomness for Cr(VI), As(III), Cd(II), and Pb(II) adsorption was observed for positive ΔS° values. The positive ΔG° value indicated that the adsorption process for Cr(VI), As(III), Cd(II), and Pb(II) was all nonspontaneous; a decrease of ΔG° value with an increasing temperature implies unfavored at a higher temperature.

Competitive Adsorption. Binary component systems were put forward to investigate the competitive adsorption between each of the two metal ions. The results showed that Pb(II) adsorption capacity was increased at first and then decreased with the increase of As(III) initial concentration (Figure 4a). Meanwhile, the As(III) adsorption capacity first rises and then descends with increasing Pb(II) initial concentration (Figure 4b). It implies that different active sites were provided for As(III) and Pb(II) ions at low initial concentrations, while the same active sites were competed by As(III) and Pb(II) ions at high initial concentrations, implying an identical affinity of adsorption sites for As(III) and Pb(II). The conclusion could equally well apply to As(III)/Cd(II) completion adsorption, as the As(III) adsorption capacity is unaffected by Cd(II) initial concentration (Figure 4f). Surprisingly, Cr(VI) adsorption capacity began to gyrate up with the increase of As(III) and Cd(II) initial concentration (Figure 4c,d), while Cd(II) adsorption capacity was decreased gradually when the Cr(VI) initial concentration was more than 20 mg L⁻¹ (Figure 4e). Cr(VI) adsorption capacity is entirely unrelated to the initial concentration of As(III) and Cd(II), while Cd(II) adsorption was suppressed by superfluous Cr(VI) ions, implying a completely different mechanism for Cr(VI) by the sulphydryl-functionalized polymer particles.

Given that multiple metal ions coexist in actual wastewater, binary component systems were designed to explore the affinity of the sulphydryl-functionalized polymer for Cr(VI), As(III), Cd(II), and Pb(II) toward the active sites of functional groups. The results of competitive adsorption showed that a unique active site for Cr(VI) adsorption was observed, and Cr(VI) would complete the active sites with Cd(II) when the concentration of Cr(VI) was >20 mg/L. However, the adsorption of Cr(VI) is not affected by the concentration of As(III), Cd(II), and Pb(II), which implies that the adsorption sites are specifically provided to Cr(VI). Interestingly, As(III), Cd(II), and Pb(II) would compete for active sites with each other, which suggests that the same active sites or a similar adsorption mechanism is for As(III), Cd(II), and Pb(II) adsorption by the sulphydryl-functionalized polymer.

Plausible Adsorption Mechanisms. Fourier transform infrared spectroscopy (FTIR) was conducted to explore the mechanism of Cr(VI), As(III), Cd(II), and Pb(II) adsorption by the sulphydryl-functionalized polymer particles from the functional groups. A new stretching peak at 528 cm⁻¹ was assigned to the –Cr–N group, and the absorbance broad peak markedly enhanced between 3500 and 3000 cm⁻¹ was attributed to the increase of the –NH– group after Cr(VI) adsorption (Figure 5).³¹ Chigondo et al. revealed that ionic interaction between –NH– group and Cr(VI) was proven for the blue shift of –NH– group at about 3000 cm⁻¹.³⁹ The decrease of benzenoid amine stretching vibration at 1508 cm⁻¹ and the increase of quinoid imine stretching vibrations at 1623 cm⁻¹ further suggested a reduction between Cr(VI) species and benzenoid amine/quinoid imine units. The relative intensity of benzenoid amine and quinoid imine does not change after As(III), Cd(II), and Pb(II) adsorption, while the relative intensity of –C–O group stretching at 1232 cm⁻¹ and –C–H stretching at 833 cm⁻¹ was significantly increased, implying that the mechanism of As(III), Cd(II), and Pb(II) adsorption are related to –C–O group and –C–H functional groups.

X-ray photoelectron spectroscopy (XPS) spectra was recorded and are shown in Figures 6 and S1 and Table S2. The content of $-\text{NH}_2$ and $-\text{SH}$ groups before adsorption is 10.23 and 10.92%, respectively. Typical Cr 2p_{3/2} and Cr 2p_{1/2} peaks indicated chromium species on the surface of the sulphydryl-functionalized polymer particles after adsorption (Figure 6c). The deconvolution of Cr 2p_{3/2} and Cr 2p_{1/2} orbitals was distributed to the peaks at 579.7 eV and 589.1 eV for Cr(VI) with molar ratios of 34.4%, and the peaks at 576.7, 577.9, 586.4, and 587.4 eV for chromium(III) at 65.6%, revealed that a major part of Cr(VI) adsorbed on the surface of the sulphydryl-functionalized polymer particles was reduced to Cr(III) species.^{31,40–42} The deconvolution of Cd 3d_{5/2} at 405.8 and 412.5 eV was assigned to Cd(OH)₂ and CdO species, and typical Cd(II) peaks were observed (Figure 6d,e), implying that precipitation for Cd(II) adsorption was convinced.⁴⁰

N species peaks were deconvoluted into benzenoid amine at 400.2 eV and quinoid imine at 399.4 eV.^{14,34} The molar ratio of benzenoid amine in the pristine sulphydryl-functionalized polymer particles was 86.8%, which decreased to 44.6, 36.4, 39.5, and 41.0% after As(III), Cr(VI), Cd(II), and Pb(II) adsorption, respectively (Figure 6). Meanwhile, the molar ratio of quinoid imine was increased from 13.2 to 55.4, 36.1, 60.5, and 59.0%, respectively, implying a redox reaction during As(III), Cr(VI), Cd(II), and Pb(II) adsorption. A new peak at 401.3 eV due to protonate quinoid imine ($-\text{N}=\text{+}$) can further confirm the reduction between the quinoid imine and benzenoid amine (Figure 6c). The SO₄²⁻ group peak at 168.1 eV can be considered to be caused by the oxidation of the $-\text{SH}$ group. That is to say, the grafted sulphydryl-functionalized group was oxidized by benzenoid amine. The increase of the molar ratio of S 2p_{3/2} at 163.7 eV from 35.4 to 43.2 and 43.2% for As(III) and Pb(II) adsorption indicated chelation between As(III)/Pb(II) and $-\text{SH}$ group,¹² while the decrease of the molar ratio of O 1s at 533.1 eV from 44.8 to 37.3 and 36.7% for Cr(VI) and Pb(II) suggest complexation between Cr(VI)/Pb(II) and C=O or benzene hydroxyl.

In summary, the adsorption capacity of As(III), Cr(VI), Cd(II), and Pb(II) by the sulphydryl-functionalized polymer is higher than part of natural materials, like *Acorus calamus*, shanghai silty clay, and Banana peel, even higher than some nanomaterial and modified absorbents, such as APTES-functionalized magnetic biochar, sulphydryl-functionalized chitosan, and nanoparticles (Table S3). The electron-donating of Cr(VI) reduced to Cr(III) originates from the benzenoid amine to quinoid imine/protonated nitrogen unit ($-\text{N}=\text{+}$), implying that Cr(VI) reduction is the predominant adsorption mechanism. Meanwhile, complexation between Cr(VI)/Pb(II) and C=O or benzene hydroxyl is plausible. The chelation between As(III)/Pb(II) and $-\text{SH}$ group is convincing.

CONCLUSIONS

In summary, we designed a sulphydryl-functionalized polymer with intrinsic amine groups to take up Cr(VI), As(III), Cd(II), and Pb(II). The high-efficiency adsorption capacity was obtained by the bifunctional adsorbent. Furthermore, 65.6% of Cr(VI) was reduced to Cr(III) species; it can be believed that the electron donor comes from the benzenoid amine, implying a unique mechanism for Cr(VI) adsorption by the sulphydryl-functionalized polymer particles. Chemisorption with electrostatic adsorption was a co-occurrence during Cr(VI) adsorption. The difference is that complexation

between Pb(II) and C=O or benzene hydroxyl and chelation between As(III)/Pb(II) and the $-\text{SH}$ group were the dominant mechanisms for As(III), Cd(II), and Pb(II) adsorption. The designed nanoporous adsorbents offer promise for efficient removal of heavy metal pollutants.

ASSOCIATED CONTENT

Supporting Information

The Supporting Information is available free of charge at <https://pubs.acs.org/doi/10.1021/acs.langmuir.3c02778>.

TEM image, XPS analysis results, thermodynamics parameters, content of functional groups, and comparison of the adsorption capacity (PDF)

AUTHOR INFORMATION

Corresponding Author

Rongtai Yu – School of Materials Science and Engineering, Jingdezhen Ceramic University, Jingdezhen, Jiangxi 333403, P. R. China; orcid.org/0000-0001-6182-6576; Email: yurongtai@jci.edu.cn

Authors

Yueyang Wang – School of Materials Science and Engineering, Jingdezhen Ceramic University, Jingdezhen, Jiangxi 333403, P. R. China

Weiwei Lu – School of Materials Science and Engineering, Jingdezhen Ceramic University, Jingdezhen, Jiangxi 333403, P. R. China

Fangfen Jing – School of Materials Science and Engineering, Jingdezhen Ceramic University, Jingdezhen, Jiangxi 333403, P. R. China

Mingzhu Jin – School of Materials Science and Engineering, Jingdezhen Ceramic University, Jingdezhen, Jiangxi 333403, P. R. China

Xinyang He – School of Materials Science and Engineering, Jingdezhen Ceramic University, Jingdezhen, Jiangxi 333403, P. R. China

Yuchen Xue – School of Materials Science and Engineering, Jingdezhen Ceramic University, Jingdezhen, Jiangxi 333403, P. R. China

Yajun Hu – School of Materials Science and Engineering, Jingdezhen Ceramic University, Jingdezhen, Jiangxi 333403, P. R. China

Complete contact information is available at: <https://pubs.acs.org/10.1021/acs.langmuir.3c02778>

Author Contributions

#Yueyang Wang and Weiwei Lu's contribution is equal, therefore, they are co-first authors.

Notes

The authors declare no competing financial interest.

ACKNOWLEDGMENTS

The authors acknowledge the financial support provided by the National Natural Science Foundation of China (S2060009).

REFERENCES

- (1) Nicholson, J. W. Etymology of 'polymers'. *Educ. Chem.* 1991, 28, 70–71.
- (2) Feldman, D. Polymer History. *Des. Monomers Polym.* 2008, 11 (1), 1–15.

- (3) Hu, J.; Zhao, X.; Zhang, G.; Cui, Z.; Wang, C. Synthesis of a “turn-on” fluorescent polymer probe, preparation and reusability of its test paper on metal ions detection. *J. Taiwan Inst. Chem. Eng.* **2023**, *142*, 104630.
- (4) Rani Sethy, T.; Biswal, T.; Kumar Sahoo, P. An indigenous tool for the adsorption of rare earth metal ions from the spent magnet e-waste: An eco-friendly chitosan biopolymer nanocomposite hydrogel. *Sep. Purif. Technol.* **2023**, *309*, 122935.
- (5) Sun, H.; Zhan, J.; Chen, L.; Zhao, Y. Preparation of CTS/PAMAM/SA/Ca²⁺ hydrogel and its adsorption performance for heavy metal ions. *Appl. Surf. Sci.* **2023**, *607*, 155135.
- (6) Zhao, G.; Huang, X.; Tang, Z.; Huang, Q.; Niu, F.; Wang, X. Polymer-based nanocomposites for heavy metal ions removal from aqueous solution: a review. *Polym. Chem.* **2018**, *9* (26), 3562–3582.
- (7) Elwakeel, K.; El-Binary, A.; Kouta, E.; Guibal, E. Functionalization of polyacrylonitrile/Na-Y zeolite composite with amidoxime groups for the sorption of Cu (II), Cd (II) and Pb (II) metal ions. *Chem. Eng. J.* **2018**, *332*, 727–736.
- (8) Wieszczycka, K.; Filipowiak, K.; Wojciechowska, I.; Aksamitowski, P. Novel ionic liquid-modified polymers for highly effective adsorption of heavy metals ions. *Sep. Purif. Technol.* **2020**, *236*, 116313.
- (9) Cumbal, L.; SenGupta, A. K. Arsenic removal using polymer-supported hydrated iron (III) oxide nanoparticles: role of Donnan membrane effect. *Environ. Sci. Technol.* **2005**, *39* (17), 6508–6515.
- (10) Zhang, Q.; Pan, B.; Chen, X.; Zhang, W.; Pan, B.; Zhang, Q.; Lv, L.; Zhao, X. Preparation of polymer-supported hydrated ferric oxide based on Donnan membrane effect and its application for arsenic removal. *Sci. China, Ser. B: Chem.* **2008**, *51* (4), 379–385.
- (11) Li, X.; Zhou, H.; Wu, W.; Wei, S.; Xu, Y.; Kuang, Y. Studies of heavy metal ion adsorption on chitosan/sulphydryl-functionalized graphene oxide composites. *J. Colloid Interface Sci.* **2015**, *448*, 389–397.
- (12) Ye, Y.; Zhang, T.; Lv, L.; Chen, Y.; Tang, W.; Tang, S. Functionalization of chitosan by grafting sulphydryl groups to intensify the adsorption of arsenite from water. *Colloids Surf., A* **2021**, *622*, 126601.
- (13) Cao, H.; Yang, P.; Ye, T.; Yuan, M.; Yu, J.; Wu, X.; Yin, F.; Li, Y.; Xu, F. Recognizing adsorption of Cd(II) by a novel core-shell mesoporous ion-imprinted polymer: Characterization, binding mechanism and practical application. *Chemosphere* **2021**, *278*, 130369.
- (14) Acharya, R.; Lenka, A.; Parida, K. Magnetite modified amino group based polymer nanocomposites towards efficient adsorptive detoxification of aqueous Cr (VI): A review. *J. Mol. Liq.* **2021**, *337*, 116487.
- (15) Liu, J.; Qiao, S. Z.; Liu, H.; Chen, J.; Orpe, A.; Zhao, D.; Lu, G. Q. M. Extension of The Stber Method to the Preparation of Monodisperse Resorcinol-Formaldehyde Resin Polymer and Carbon Spheres. *Angew. Chem.* **2011**, *123*, 6069–6073.
- (16) Dong, Y.-R.; Nishiyama, N.; Egashira, Y.; Ueyama, K. Basic Amid Acid-Assisted Synthesis of Resorcinol-Formaldehyde Polymer and Carbon Nanospheres. *Ind. Eng. Chem. Res.* **2008**, *47* (14), 4712–4716.
- (17) Liu, M.; Cai, C.; Li, J.; Zhao, J.; Teng, W.; Liu, R. Stöber synthesis of tannic acid-formaldehyde resin polymer spheres and their derived carbon nanospheres and nanocomposites for oxygen reduction reaction. *J. Colloid Interface Sci.* **2018**, *528*, 1–9.
- (18) Liu, J.; Wickramaratne, N. P.; Qiao, S. Z.; Jaroniec, M. Molecular-based design and emerging applications of nanoporous carbon spheres. *Nat. Mater.* **2015**, *14* (8), 763–774.
- (19) Ambika, S.; Kumar, M.; Pisharody, L.; Malhotra, M.; Kumar, G.; Sreedharan, V.; Singh, L.; Nidheesh, P. V.; Bhatnagar, A. Modified biochar as a green adsorbent for removal of hexavalent chromium from various environmental matrices: Mechanisms, methods, and prospects. *Chem. Eng. J.* **2022**, *439*, 135716.
- (20) Arora, R. Adsorption of Heavy Metals-A Review. *Mater. Today* **2019**, *18*, 4745–4750.
- (21) Priya, A. K.; Jalil, A. A.; Vadivel, S.; Dutta, K.; Rajendran, S.; Fujii, M.; Soto-Moscoso, M. Heavy metal remediation from wastewater using microalgae: Recent advances and future trends. *Chemosphere* **2022**, *305*, 135375.
- (22) Zahra, M. H.; Hamza, M. F.; El-Habibi, G.; Abdel-Rahman, A. A. H.; Mira, H. I.; Wei, Y.; Alotaibi, S. H.; Amer, H. H.; Goda, A. E. S.; Hamad, N. A. Synthesis of a Novel Adsorbent Based on Chitosan Magnetite Nanoparticles for the High Sorption of Cr (VI) Ions: A Study of Photocatalysis and Recovery on Tannery Effluents. *Catalysts* **2022**, *12*, 678.
- (23) Kumarage, S.; Munaweera, I.; Sandaruwan, C.; Weerasinghe, L.; Kotegoda, N. Electrospun amine-functionalized silica nanoparticles-cellulose acetate nanofiber membranes for effective removal of hardness and heavy metals (As(V), Cd(II), Pb(II)) in drinking water sources. *Environ. Sci.: Water Res. Technol.* **2023**, *9* (10), 2664–2679.
- (24) Yu, R.; Huang, X.; Liu, Y.; Kong, Y.; Gu, Z.; Yang, Y.; Wang, Y.; Ban, W.; Song, H.; Yu, C. Shaping Nanoparticles for Interface Catalysis: Concave Hollow Spheres via Deflation-Inflation Asymmetric Growth. *Adv. Sci.* **2020**, *7* (13), 2000393.
- (25) He, X.; Deng, F.; Shen, T.; Yang, L.; Chen, D.; Luo, J.; Luo, X.; Min, X.; Wang, F. Exceptional adsorption of arsenic by zirconium metal-organic frameworks: Engineering exploration and mechanism insight. *J. Colloid Interface Sci.* **2019**, *539*, 223–234.
- (26) Sips, R. On the Structure of a Catalyst Surface. *J. Chem. Phys.* **1948**, *16* (5), 490–495.
- (27) Wu, F.-C.; Tseng, R.-L.; Juang, R.-S. Characteristics of Elovich equation used for the analysis of adsorption kinetics in dye-chitosan systems. *Chem. Eng. J.* **2009**, *150* (2–3), 366–373.
- (28) Wang, J.; Zhang, W. Evaluating the adsorption of Shanghai silty clay to Cd(II), Pb(II), As(V), and Cr(VI): kinetic, equilibrium, and thermodynamic studies. *Environ. Monit. Assess.* **2021**, *193* (3), 131.
- (29) Chang, X.; Li, M.; Liu, Q.; Liu, Q.; Yao, J. Adsorption-reduction of chromium(VI) from aqueous solution by phenol-formaldehyde resin microspheres. *RSC Adv.* **2016**, *6* (52), 46879–46888.
- (30) Bin, D. S.; Chi, Z. X.; Li, Y.; Zhang, K.; Yang, X.; Sun, Y. G.; Piao, J. Y.; Cao, A. M.; Wan, L. J. Controlling the Compositional Chemistry in Single Nanoparticles for Functional Hollow Carbon Nanospheres. *J. Am. Chem. Soc.* **2017**, *139* (38), 13492–13498.
- (31) Jin, L.; Huang, L.; Ren, L.; He, Y.; Tang, J.; Wang, S.; Yang, W.; Wang, H.; Chai, L. Preparation of stable and high-efficient poly(m-phenylenediamine)/reduced graphene oxide composites for hexavalent chromium removal. *J. Mater. Sci.* **2019**, *54* (1), 383–395.
- (32) Chai, L.; Wang, T.; Zhang, L.; Wang, H.; Yang, W.; Dai, S.; Meng, Y.; Li, X. A Cu-m-phenylenediamine complex induced route to fabricate poly (m-phenylenediamine)/reduced graphene oxide hydrogel and its adsorption application. *Carbon* **2015**, *81*, 748–757.
- (33) Das, T. K.; Sakthivel, T. S.; Jeyaranjan, A.; Seal, S.; Bezbaruah, A. N. Ultra-high arsenic adsorption by graphene oxide iron nanohybrid: Removal mechanisms and potential applications. *Chemosphere* **2020**, *253*, 126702.
- (34) Wang, T.; Zhang, L.; Li, C.; Yang, W.; Song, T.; Tang, C.; Meng, Y.; Dai, S.; Wang, H.; Chai, L.; et al. Synthesis of Core-Shell Magnetic Fe₃O₄@poly(m-Phenylenediamine) Particles for Chromium Reduction and Adsorption. *Environ. Sci. Technol.* **2015**, *49* (9), 5654–5662.
- (35) Jain, M.; Yadav, M.; Kohout, T.; Lahtinen, M.; Garg, V. K.; Sillanpää, M. Development of iron oxide/activated carbon nanoparticle composite for the removal of Cr(VI), Cu(II) and Cd(II) ions from aqueous solution. *Water Resour. Ind.* **2018**, *20*, 54–74.
- (36) Wang, J.; Chen, N.; Li, M.; Feng, C. Efficient Removal of Fluoride Using Polypyrrole-Modified Biochar Derived from Slow Pyrolysis of Pomelo Peel: Sorption Capacity and Mechanism. *J. Polym. Environ.* **2018**, *26* (4), 1559–1572.
- (37) Al-Ghouti, M. A.; Da'ana, D. A. Guidelines for the use and interpretation of adsorption isotherm models: A review. *J. Hazard. Mater.* **2020**, *393*, 122383.
- (38) Ahmad, Z. U.; Yao, L.; Wang, J.; Gang, D. D.; Islam, F.; Lian, Q.; Zappi, M. E. Neodymium embedded ordered mesoporous carbon (OMC) for enhanced adsorption of sunset yellow: Characterizations,

adsorption study and adsorption mechanism. *Chem. Eng. J.* **2019**, *359*, 814–826.

(39) Chigondo, M.; Paumo, H. K.; Bhaumik, M.; Pillay, K.; Maity, A. Magnetic arginine-functionalized polypyrrole with improved and selective chromium (VI) ions removal from water. *J. Mol. Liq.* **2019**, *275*, 778–791.

(40) Herath, A.; Layne, C. A.; Perez, F.; Hassan, E. B.; Pittman, C. U., Jr; Mlsna, T. E. KOH-activated high surface area Douglas Fir biochar for adsorbing aqueous Cr(VI), Pb(II) and Cd(II). *Chemosphere* **2021**, *269*, 128409.

(41) Sun, Y.; Yu, F.; Li, L.; Ma, J. Adsorption-reduction synergistic effect for rapid removal of Cr (VI) ions on superelastic NH₂-graphene sponge. *Chem. Eng. J.* **2021**, *421*, 129933.

(42) Zhu, D.; Shao, J.; Li, Z.; Yang, H.; Zhang, S.; Chen, H. Nano nickel embedded in N-doped CNTs-supported porous biochar for adsorption-reduction of hexavalent chromium. *J. Hazard. Mater.* **2021**, *416*, 125693.